

## Article

# Polarization Spectroscopy Applied to Electromagnetically Induced Transparency in Hot Rydberg Atoms Using a Laguerre–Gaussian Beam

Naomy Duarte Gomes<sup>1</sup> , Bárbara da Fonseca Magnani<sup>1</sup> , Jorge Douglas Massayuki Kondo<sup>2</sup>   
and Luis Gustavo Marcassa<sup>1,\*</sup> 

<sup>1</sup> Instituto de Física de São Carlos, Universidade de São Paulo, Caixa Postal 369, São Carlos 13560-970, SP, Brazil; naomy.gomes@usp.br (N.D.G.); barbara.f.magnani@gmail.com (B.d.F.M.)

<sup>2</sup> Departamento de Física, Universidade Federal de Santa Catarina, Florianópolis 88040-900, SC, Brazil; massayuki.kondo@ufsc.br

\* Correspondence: marcassa@ifsc.usp.br

**Abstract:** In this work, we have applied polarization spectroscopy to study electromagnetically induced transparency involving hot <sup>85</sup>Rb Rydberg state in a vapor cell using a Laguerre–Gaussian mode beam. Such spectroscopy technique generates a dispersive signal, which allows a direct measurement of the transition linewidth. Our results show that the measured transition linewidth for a Laguerre–Gaussian mode control beam is narrower than for a Gaussian mode. Besides, it can be well reproduced by a simplified Lindblad master equation model.

**Keywords:** electromagnetically induced transparency; Laguerre–Gaussian modes; rydberg atoms



**Citation:** Duarte Gomes, N.; da Fonseca Magnani, B.; Massayuki Kondo, J.D.; Marcassa, L.G. Polarization Spectroscopy Applied to Electromagnetically Induced Transparency in Hot Rydberg Atoms Using a Laguerre–Gaussian Beam. *Atoms* **2022**, *10*, 58. <https://doi.org/10.3390/atoms10020058>

Academic Editors: José Tito Mendonça and Hugo Terças

Received: 26 April 2022

Accepted: 27 May 2022

Published: 1 June 2022

**Publisher's Note:** MDPI stays neutral with regard to jurisdictional claims in published maps and institutional affiliations.



**Copyright:** © 2022 by the authors. Licensee MDPI, Basel, Switzerland. This article is an open access article distributed under the terms and conditions of the Creative Commons Attribution (CC BY) license (<https://creativecommons.org/licenses/by/4.0/>).

## 1. Introduction

Electromagnetically induced transparency (EIT) is a nonlinear optical phenomenon, which occurs in three-level atomic systems [1,2]. The medium, which is opaque to a weak probe electromagnetic field, may become transparent due to a strong control electromagnetic field. It is characterized by the modification of the absorption profile as well by significant reduction of the light speed [3], thus increasing light–matter interaction time.

The excited electron in a Rydberg atom is very loosely bound to its ionic core, so Rydberg atoms exhibit exaggerated properties [4,5]. Among them, it is very high polarizability, which makes them very sensitive to electromagnetic fields and interactions with another Rydberg atom [6,7]. Such systems are perfect to be probed by EIT [8,9], and they are particularly attractive for quantum technologies [10–14]. EIT can also be used with Rydberg atoms to map interactions between those atoms to photon–photon interactions [15,16]. Another interesting application of the combination EIT–Rydberg atoms is the growing field of microwave and radio-frequency measurements [17–22]. All these Rydberg research areas require the ability to detect small changes in the EIT linewidth. Therefore, the development of experimental techniques which can produce narrower linewidths in Rydberg EIT is timely.

The combination of a spatially varying optical field and EIT is of considerable interest. The Laguerre–Gaussian (LG) mode [23], which presents a cylindrical symmetric intensity profile, is a perfect candidate for such a field. Its spatial dependence intensity, which reduces to zero at the center, and orbital angular momentum (OAM) of  $l\hbar$  per photon are of considerable interest for quantum computing [24], communication systems [25], forbidden transitions [26] and confinement of Rydberg atoms [27]. It was also shown that the LG mode can narrow the EIT full width at half maximum (FWHM) in a three-level lambda configuration when compared to a Gaussian mode in a hot Rb atomic vapor [28–30] and ultracold Rb [31,32].

Polarization spectroscopy (PS) is a very sensitive Doppler free technique, which produces a dispersive absorption profile with a good signal to noise ratio. It has been used to investigate excited states [33] and also to stabilize laser for Rydberg transitions [34]. Its main advantage over dichroic atomic vapor spectroscopy (DAVS) is that it does not require a magnetic field [35,36]. In this work, we have studied EIT on a three-level ladder Rydberg system in an Rb vapor cell using the PS technique for Gaussian and  $LG_0^1$  mode control beams. Its main advantage is that it allows a direct measurement of the EIT linewidth without relying on the peak-height determination. We have measured it for both modes, at the same Rabi frequency, and compared the results obtained to a simplified Lindblad master equation model, which was able to reproduce well the experimental observations. To our knowledge, this is the first work to apply an  $LG_0^1$  mode in a Rydberg EIT and observe narrowing of the transmission linewidth. This may allow better microwave and radio-frequency field measurements [17–22].

## 2. Materials and Methods

Figure 1a shows the three-level ladder Rydberg system using the  $40D$  Rydberg state. The linearly polarized probe beam, with linewidth  $\gamma_p = 1$  MHz, scans across the  $^{85}\text{Rb}$   $5S_{1/2}(F = 3) \rightarrow 5P_{3/2}(F' = 4)$  transition at 780 nm with detuning  $\Delta_p$  and Rabi frequency  $\Omega_p$ . A strong circularly polarized control beam with linewidth  $\gamma_c = 1$  MHz drives the  $5P_{3/2}(F' = 4) \rightarrow 40D_{5/2}$  transition at 480 nm, with detuning  $\Delta_c$  and Rabi frequency  $\Omega_c$ . The intermediate and the Rydberg states have natural linewidths  $\Gamma_2/2\pi = 6.06$  MHz and  $\Gamma_3/2\pi = 0.2$  kHz, respectively.

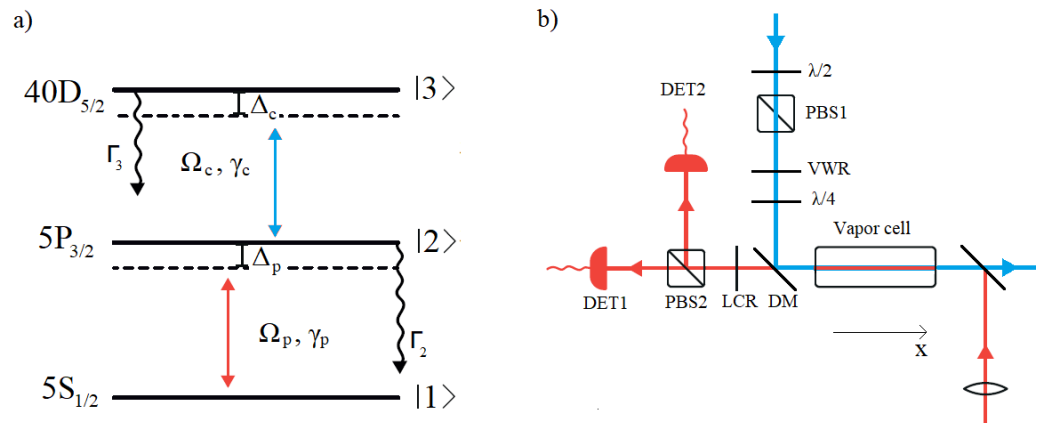


**Figure 1.** (a) Rubidium energy-level scheme for the three-level ladder Rydberg system using the  $40D_{5/2}$  Rydberg state. Relevant experimental parameters: (i) Laser linewidths ( $\gamma_p, \gamma_c$ ), detunings ( $\Delta_p, \Delta_c$ ) and Rabi frequencies ( $\Omega_p$  and  $\Omega_c$ ) for probe and control beam, respectively; (ii) Intermediate state natural linewidth  $\Gamma/2\pi = 6.06$  MHz. (b) Experimental setup: Waveplates ( $\lambda/2$  and  $\lambda/4$ ); Polarizing beam splitter (PBS1 and PBS2); Dichroic mirror (DM); Zero-order vortex half wave retarder (VWR); Liquid crystal retarder (LCR); vapor cell and photodiodes (DET1 and DET2). Probe laser (red) enters the vapor cell from the right. Control beam (blue) enters the cell from the left and overlaps with the probe beam. The probe beam transmission is detected by photodiodes.

The experimental setup is shown in Figure 1b. The probe and control laser beams are counterpropagating in a 7.5 cm long Rb vapor cell, which is kept at room temperature. A dichroic mirror is used to separate them and analyze the probe beam. Both beams are spatially filtered using single mode optical fibers in order to obtain a Gaussian beam, and they are focused at the center of the cell, which is not magnetically shielded. The probe laser has a total power of  $3.5 \mu\text{W}$  with a  $1/e^2$  waist of  $170 \pm 5 \mu\text{m}$  (Rayleigh length  $z_R \approx 116$  mm), which corresponds to a calculated  $\Omega_p/2\pi = 2.0$  MHz. The control laser is locked to a WS7 wavemeter, from High Finesse. Its maximum power is 60 mW with a  $1/e^2$  waist of  $190 \pm 5 \mu\text{m}$  (Rayleigh length  $z_R \approx 236$  mm), for both Gaussian and  $LG_0^1$  modes.

A zero-order vortex half wave retarder (VWR), Thorlabs model WPV10L-405, is used to generate the  $LG_0^1$  mode with an efficiency of 97%. The control beam power is varied by a half-wave plate and a polarizing beam splitter (PBS1). After the dichroic mirror, the probe beam passes through a half-wave liquid crystal retarder (LCR), Thorlabs model LCC1111-B, and a PBS2, which decomposes it into two orthogonal linearly polarized beams. Each beam is detected by a photodiode (DET1 and DET2), and their signals are subtracted, resulting in a dispersive signal that is due to the anisotropy generated in the atomic medium by the control beam [33]. This dispersive signal is the PS signal. The LCR is ideal for this task because it allows a precise balance of the final signal, since it does not have moving parts. To increase the signal-to-noise ratio, the control beam is modulated at 1 kHz and the detected signal is processed by a lock-in amplifier.

### 3. Theoretical Model

The atomic system is a three-level ladder, which is composed of levels  $|1\rangle$ ,  $|2\rangle$  and  $|3\rangle$ , as shown in Figure 1a. The  $|1\rangle$  and  $|2\rangle$  levels are coupled by a weak probe laser, characterized by  $\omega_p$  and  $\Delta_p$ . A strong control laser, characterized by  $\omega_c$  and  $\Delta_c$ , couples the levels  $|2\rangle$  and  $|3\rangle$ . We use a density matrix approach to model the atomic system [1] with a Lindblad master equation for the density matrix  $\rho$  given by:

$$\dot{\rho} = \frac{i}{\hbar}[\rho, H] + \mathcal{L}_\Gamma(\rho) + \mathcal{L}_{deph}(\rho), \tag{1}$$

where

$$H = \frac{\hbar}{2} \begin{bmatrix} 0 & \Omega_p & 0 \\ \Omega_p & -2\Delta_p & \Omega_c \\ 0 & \Omega_c & -2(\Delta_p + \Delta_c) \end{bmatrix} \tag{2}$$

is the perturbed Hamiltonian of the atom–light system in the rotating wave approximation. The  $\mathcal{L}_\Gamma$  and  $\mathcal{L}_{deph}$  terms account for spontaneous emission and atomic coherence dephasing due to the finite laser linewidths, respectively. The  $\mathcal{L}_\Gamma$  term is given by:

$$\mathcal{L}_\Gamma = \begin{bmatrix} \Gamma_2\rho_{22} & -\gamma_{12}\rho_{12} & -\gamma_{13}\rho_{13} \\ -\gamma_{21}\rho_{21} & \Gamma_3\rho_{33} - \Gamma_2\rho_{22} & -\gamma_{23}\rho_{23} \\ -\gamma_{31}\rho_{31} & -\gamma_{32}\rho_{32} & -\Gamma_3\rho_{33} \end{bmatrix}, \tag{3}$$

where  $\gamma_{ij} = (\Gamma_i + \Gamma_j)/2$  and  $\Gamma_{i,j}$  are the decay rate due to spontaneous emission, which in our model are  $\Gamma_1 = 0$ ,  $\Gamma_2/2\pi = 6.06$  MHz and  $\Gamma_3/2\pi = 0.2$  kHz. The  $\mathcal{L}_{deph}$  term can be written as:

$$\mathcal{L}_{deph} = \begin{bmatrix} 0 & -\gamma_p\rho_{12} & -\gamma_{rel}\rho_{13} \\ -\gamma_p\rho_{21} & 0 & -\gamma_c\rho_{23} \\ -\gamma_{rel}\rho_{31} & -\gamma_c\rho_{32} & 0 \end{bmatrix}, \tag{4}$$

where  $\gamma_{rel} = \gamma_p + \gamma_c$  is the linewidth of the two-photon resonance [37].

According to refs. [28,31],  $z$  is considered smaller than the Rayleigh length ( $z < z_R$ ), so that a plane-wave approximation can be done. Therefore, the probe and control Gaussian field amplitude are, respectively,

$$\mathcal{E}_{p,G} = \mathcal{E}_{0,p}, \tag{5a}$$

$$\mathcal{E}_{c,G} = \mathcal{E}_{0,c}, \tag{5b}$$

and for the control  $LG_0^1$  field,

$$\mathcal{E}_{c,LG} = \mathcal{E}_{0,c} \frac{r\sqrt{2}}{w_0} \exp\left(\frac{-r^2}{w_c^2}\right), \tag{6}$$

where  $r$  is the radial distance from the center axis of the beam and  $w_c$  is the  $1/e^2$  waist of the control beam. Considering the Gaussian field amplitude as constant does not affect the results to the precision of the experiment and, as demonstrated by Anupryia and

co-workers [28], the LG mode dependency on the phase factor does not affect the profile of EIT spectrum. The probe laser Rabi frequency is then given by:

$$\Omega_p = \frac{\mu_{12}\mathcal{E}_{0,p}}{\hbar}, \tag{7}$$

where  $\mu_{12}$  is the dipole moment of the  $|1\rangle \rightarrow |2\rangle$  transition. The control laser Rabi frequency, for the Gaussian mode, is:

$$\Omega_{c,G} = \frac{\mu_{23}\mathcal{E}_{0,c}}{\hbar} = \Omega_{0,c}, \tag{8}$$

where  $\mu_{23}$  is the dipole moment of the  $|2\rangle \rightarrow |3\rangle$  transition. For the  $LG_0^1$  mode, the control Rabi frequency reads:

$$\Omega_{c,LG} = \frac{\mu_{23}\mathcal{E}_{c,LG}}{\hbar} = \Omega_{0,c} \frac{\sqrt{2}r}{w_c} e^{-r^2/w_c^2}, \tag{9}$$

where  $\mathcal{E}_{c,LG}$  is given by Equation (6).

The atomic motion in the thermal vapor, at the direction of the laser beams ( $x$  axis in Figure 1b), must be taken into account. Let us consider  $v_x$  as the atomic velocity,  $k_p$  and  $k_c$  as the magnitude of the probe and control laser wave vectors, respectively. The Doppler effect modifies the laser detunings such that  $\Delta_p \rightarrow \Delta_p + k_p v_x$  and  $\Delta_c \rightarrow \Delta_c - k_c v_x$ . Equation (1) leads to the Optical Bloch Equations (OBE) for the populations ( $\rho_{ii}$ ) and coherence terms ( $\rho_{ji}$ ) of the density matrix. The OBEs can be solved analytically in the steady-state by first order perturbation theory for  $\Omega_p \ll \Omega_c$ . This condition is equivalent to assume  $\rho_{11} \sim 1$ ,  $\rho_{22} = \rho_{33} = 0$  and  $\rho_{23} = 0$ , which allow us to calculate the matrix element  $\rho_{12}$ . This term is related to the susceptibility,

$$\rho_{12} = \frac{i\Omega_p/2}{\frac{\Omega_c^2/4}{\Gamma_3/2 + \gamma_{rel} - i(\Delta_p + k_p v_x + \Delta_c - k_c v_x)} + \Gamma_2/2 + \gamma_p - i(\Delta_p + k_p v_x)}, \tag{10}$$

where  $\Omega_c$  is given by either Equation (8) or (9), depending on the control beam mode. The Doppler averaged susceptibility allows us to calculate the probe beam transmission ( $Tr_p$ ):

$$\chi = \frac{2N|\mu_{12}|^2}{\hbar\epsilon_0\Omega_p\sqrt{\pi}u} \int_{-\infty}^{+\infty} \rho_{12} e^{-v^2/u^2} dv, \tag{11}$$

where  $N$  is the atomic vapor density, and  $u = \sqrt{2k_B T/m}$  is the root-mean square velocity at a given temperature  $T$  and  $m$  is the atomic mass. Therefore, the probe beam transmission for a Gaussian mode through the vapor cell, with length  $l$ , can be written as:

$$Tr_p = e^{-Im[\chi]k_p l}. \tag{12}$$

For the  $LG_0^1$  mode, the transmission must be integrated over the EIT region. Akin and co-workers have proposed that such integral should be performed over a circle with a radius equals to the probe waist  $w_p$  [31]. Therefore, the transmission becomes:

$$Tr_p = \frac{2}{w_p^2} \int_0^{w_p} \exp(-Im[\chi]k_p l) r dr. \tag{13}$$

Carr and co-workers have proposed that the PS signal ( $S$ ) is proportional to the real part of the susceptibility ( $\chi$ ) [33]. For the Gaussian mode control beam, the signal is given by:

$$S_G = \frac{k_p}{2} Re[\chi], \tag{14}$$

where  $\Omega_c$  is given by Equation (8). For the  $LG_0^1$  mode, the susceptibility must again be integrated over the EIT region, and the PS signal can be written as:

$$S_{LG} = \frac{2}{w_p^2} \int_0^{w_p} \frac{k_p}{2} \text{Re}[\chi] r dr. \quad (15)$$

#### 4. Results and Discussions

Figure 2 shows EIT transmission spectra for a Gaussian control beam as a function of  $\Delta_p$ , for  $\Delta_c = 0$  and  $\Omega_{0,c}/2\pi = 4.6$  MHz. The full red line was obtained using a single photodiode corresponding to the probe beam transmission, while the black line is the PS signal. We have defined the frequency difference between the valley and the peak, in the PS signal, as  $\Delta\omega_G$  for the Gaussian mode control beam. We find the valley and the peak using the *scipy.signal* function *argrextrema* [38], which calculates the relative extrema of the data, returning their position the  $x$ -axis. We have verified theoretically and experimentally that parameter  $\Delta\omega$  is equal to the FWHM of the single photodiode signal.

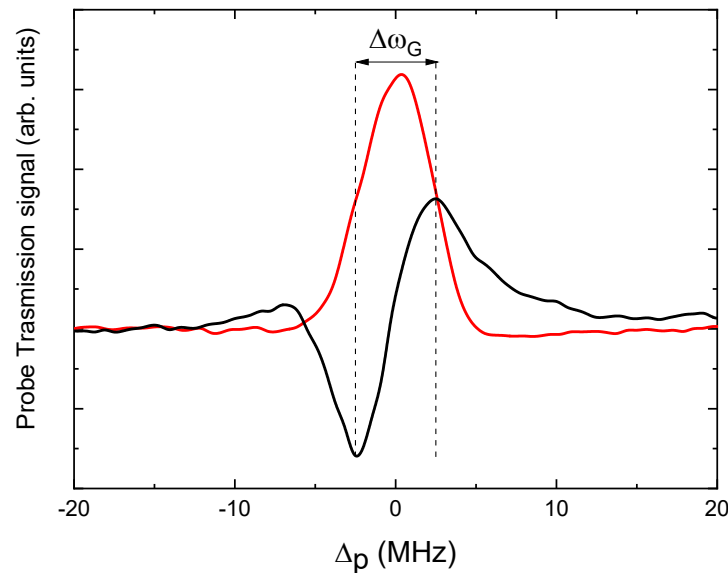
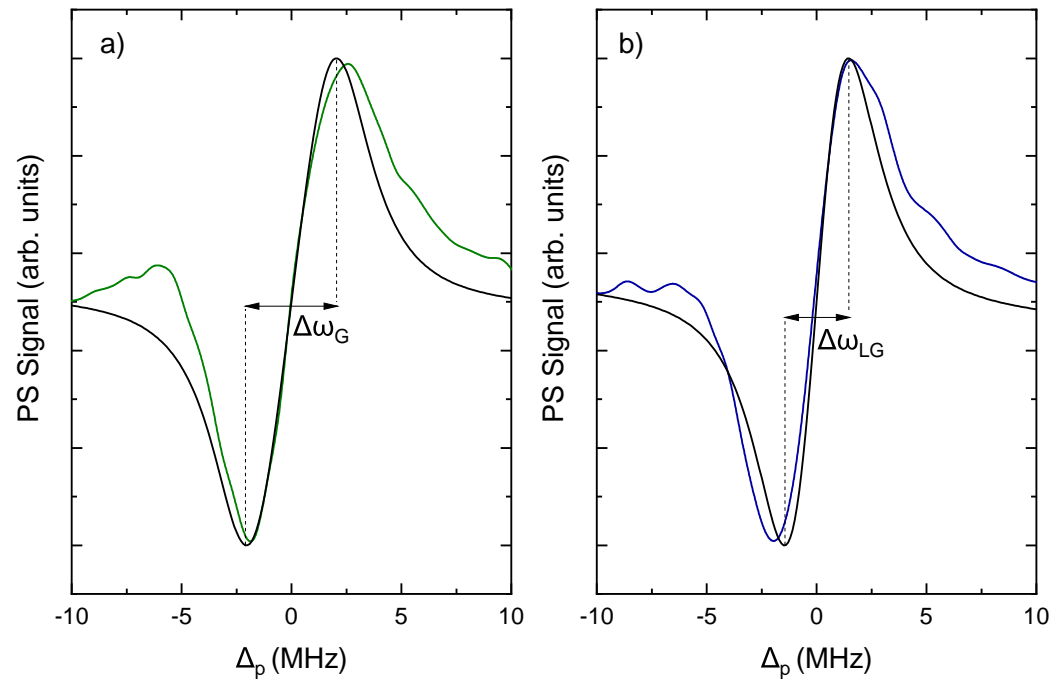


**Figure 2.** Probe laser transmission, with Gaussian mode control beam. The red line is the signal obtained with a single photodiode, which shows the EIT Lorentzian transmission profile. The black line was obtained with the PS technique. The  $^{85}\text{Rb } 5S_{1/2}(F = 3) \rightarrow 5P_{3/2}(F' = 4)$  transition is set to  $\Delta_p = 0$  MHz. For both curves,  $\Omega_c/2\pi = 4.87$  MHz and  $\Delta_c = 0$  MHz. The frequency difference between the valley and the peak of the PS signal is  $\Delta\omega_G$  for the Gaussian mode.

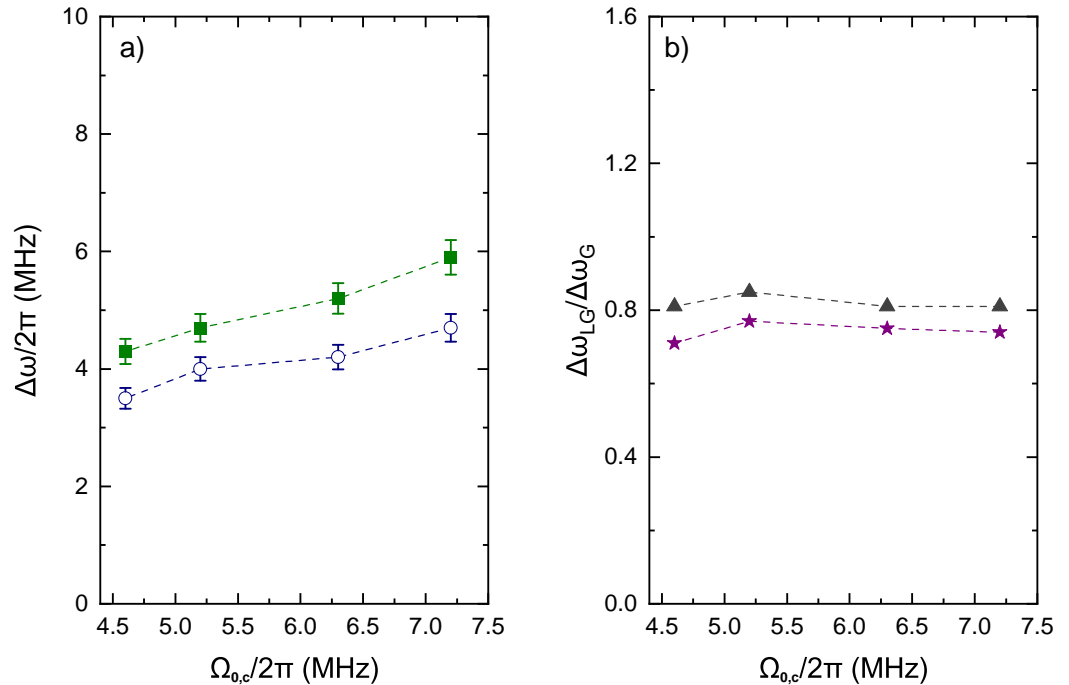
Figure 3 shows the experimental PS spectra (colored lines) as a function of  $\Delta_p$  for a Gaussian (Figure 3a—green line) and  $LG_0^1$  (Figure 3b—blue line) mode control beams. The black lines are the theoretical model, considering  $\Omega_{0,c}/2\pi = 4.6$  MHz,  $\Delta_c = 0$  and  $N \sim 1 \times 10^{-10} \text{ cm}^3$ . In this case, we have measured  $\Delta\omega_G/2\pi = 4.3 \pm 0.2$  MHz and  $\Delta\omega_{LG}/2\pi = 3.5 \pm 0.2$  MHz for the Gaussian and  $LG_0^1$  mode, respectively.

Figure 4a shows the experimental  $\Delta\omega$  as a function of  $\Omega_{0,c}$  for Gaussian (green squares) and  $LG_0^1$  (open blue circles) control beams. Figure 4b shows the  $\Delta\omega_{LG}/\Delta\omega_G$  as a function of  $\Omega_{0,c}$  for experimental data (gray triangles) and theoretical models (purple stars).

The PS technique produces a dispersive absorption profile and allows the direct width measurement without relying on the peak height determination. All the experimental linewidths are narrower than the natural linewidth of  $5P_{3/2}$  state, especially when the  $LG_0^1$  mode control beam is used.



**Figure 3.** Experimental PS signal as a function of  $\Delta_p$  for: (a) Gaussian (green line) and (b)  $LG_0^1$  (blue line) control beams. The black lines are the theoretical prediction considering  $\Omega_{0,c}/2\pi = 4.6$  MHz and  $\Delta_c = 0$ . For these parameters, the observed widths are  $\Delta\omega_G/2\pi = 4.3 \pm 0.2$  MHz and  $\Delta\omega_{LG}/2\pi = 3.5 \pm 0.2$  MHz, showing the decrease of the width when the probe is in the  $LG_0^1$  mode.



**Figure 4.** (a) Experimental  $\Delta\omega$  as a function of  $\Omega_{0,c}$  for Gaussian (green squares) and  $LG_0^1$  (open blue circles) control beams. (b)  $\Delta\omega_{LG}/\Delta\omega_G$  as a function of  $\Omega_{0,c}$  for experimental data (gray triangles) and theoretical model (purple stars). The dashed lines here are for guidance.

The results show that the PS signal width, for the Gaussian mode, is always larger than the  $LG_0^1$  mode. In the studied Rabi frequency range, this difference is about 20%. Although the linewidth varies as a function of  $\Omega_{0,c}$ , the  $\Delta\omega_{LG}/\Delta\omega_G$  seems to be constant, indicating that both linewidths present the same  $\Omega_{0,c}$  dependence. The narrowing occurs due to the

spatial dependence of the  $LG_0^1$  mode, which causes its overall Rabi frequency to be lower at the center of the probe beam.

Experimental data and the theoretical model agree, with theory predicting widths on average 13% smaller and the ratios  $\Delta\omega_{LG}/\Delta\omega_G$  to be on average 9.6% smaller than the ratios measured. A better quantitative agreement would require the model to incorporate effects that broaden the widths, such as a Doppler mismatch between the two wavelengths, collisions, transit time, external fields and magnetic sublevels [39,40].

## 5. Conclusions

In this paper, we have implemented a polarization spectroscopy technique to study EIT on Rydberg atoms in a vapor cell, using Gaussian and  $LG_0^1$  mode control beams. Both modes present sub-natural linewidths, but the  $LG_0^1$  mode produces narrower widths when compared to the Gaussian mode with the same peak intensity. The PS technique is very convenient because it allows a direct measurement of such widths. A simplified three-level ladder system density matrix approach presents good agreement with the experimental results and it gives an insight into the role of the  $LG_0^1$  mode. The developed technique has the potential to improve the observation of several effects involving hot and cold Rydberg atoms [6–22], which require a narrower linewidth. The results presented here may be improved by optimization of magnetic field, probe laser intensity and optical density [41].

**Author Contributions:** Conceptualization, N.D.G. and L.G.M.; methodology, N.D.G., B.d.F.M., J.D.M.K. and L.G.M.; software, N.D.G.; validation, N.D.G. and L.G.M.; formal analysis, N.D.G. and L.G.M.; investigation, N.D.G. and L.G.M.; resources, L.G.M.; data curation, N.D.G. and L.G.M.; writing—original draft preparation, N.D.G. and L.G.M.; writing—review and editing, N.D.G., B.d.F.M., J.D.M.K. and L.G.M.; visualization, N.D.G.; supervision, L.G.M.; project administration, L.G.M.; funding acquisition, L.G.M. All authors have read and agreed to the published version of the manuscript.

**Funding:** This work is supported by grants 2016/21311-2, 2019/10971-0 and 2021/06371-7, São Paulo Research Foundation (FAPESP), and CNPq. It was supported by Army Research Office—Grant Number W911NF-21-1-0211.

**Institutional Review Board Statement:** Not applicable.

**Informed Consent Statement:** Not applicable.

**Data Availability Statement:** The data collected are available in the repository of the Photonics Group of the University of São Paulo and can be accessed at <https://fotonica.ifsc.usp.br/pagina/home/repository> (accessed on 25 April 2022).

**Conflicts of Interest:** The authors declare no conflict of interest.

## Abbreviations

The following abbreviations are used in this manuscript:

EIT	Electromagnetically induced transparency
LG	Laguerre–Gaussian
OAM	Orbital Angular Momentum
PS	Polarization Spectroscopy
FWHM	Full width at half maximum
DAVS	Dichroic Atomic Vapor Spectroscopy
PSB	Polarizing beam splitter
LCR	Liquid crystal retarder
OBE	Optical Bloch Equations
DM	dichroic mirror
VWR	Zero-order vortex half wave retarder

## References

1. Fleischhauer, M.; Imamoglu, A.; Marangos, J.P. Electromagnetically induced transparency: Optics in coherent media. *Rev. Mod. Phys.* **2005**, *77*, 633–673. [[CrossRef](#)]
2. Marangos, J.P. Electromagnetically induced transparency. *J. Mod. Opt.* **1998**, *45*, 471–503. [[CrossRef](#)]
3. Hau, L.V.H.; Harris, S.E.; Dutton, Z.; Behroozi, C.H. Light speed reduction to 17 metres per second in an ultracold atomic gas. *Nature* **1999**, *397*, 594–598. [[CrossRef](#)]
4. Gallagher, T.F. *Rydberg Atoms*; Cambridge University Press: Cambridge, UK, 2005; Number 3.
5. Gallagher, T.F. Rydberg atoms. *Rep. Prog. Phys.* **1988**, *51*, 143–188. [[CrossRef](#)]
6. Marcassa, L.G.; Shaffer, J.P. *Advances in Atomic, Molecular and Optical Physics, Advances in Atomic, Molecular, and Optical Physics*; Arimondo, E., Berman, P.R., Lin, C.C., Eds.; Academic: New York, NY, USA, 2014; Volume 63, p. 47.
7. Jones, M.P.; Marcassa, L.G.; Shaffer, J. Special issue on cold Rydberg atoms. *J. Phys. At. Mol. Opt. Phys.* **2015**, *48*, 180201. [[CrossRef](#)]
8. Clarke, J.; Chen, H.; van Wijngaarden, W.A. Electromagnetically induced transparency and optical switching in a rubidium cascade system. *Appl. Opt.* **2001**, *40*, 2047–2051. [[CrossRef](#)]
9. Mohapatra, A.K.; Jackson, T.R.; Adams, C.S. Coherent Optical Detection of Highly Excited Rydberg States Using Electromagnetically Induced Transparency. *Phys. Rev. Lett.* **2007**, *98*, 113003. [[CrossRef](#)]
10. Mohapatra, A.K.; Bason, M.G.; Butscher, B.; Weatherill, K.J.; Adams, C.S. A giant electro-optic effect using polarizable dark states. *Nat. Phys.* **2008**, *4*, 890–894. [[CrossRef](#)]
11. Tauschinsky, A.; Thijssen, R.M.T.; Whitlock, S.; van Linden van den Heuvell, H.B.; Spreeuw, R.J.C. Spatially resolved excitation of Rydberg atoms and surface effects on an atom chip. *Phys. Rev. A* **2010**, *81*, 063411. [[CrossRef](#)]
12. Petrosyan, D.; Otterbach, J.; Fleischhauer, M. Electromagnetically Induced Transparency with Rydberg Atoms. *Phys. Rev. Lett.* **2011**, *107*, 213601. [[CrossRef](#)] [[PubMed](#)]
13. Firstenberg, O.; Adams, C.S.; Hofferberth, S. Nonlinear quantum optics mediated by Rydberg interactions. *J. Phys. B At. Mol. Opt. Phys.* **2016**, *49*, 152003. [[CrossRef](#)]
14. Kim, B.; Chen, K.-T.; Hsiao, S.-S.; Wang, S.-Y.; Li, K.-B.; Ruseckas, J.; Juzeliūnas, G.; Kirova, T.; Auzinsh, M.; Chen, Y.-C.; et al. A weakly-interacting many-body system of Rydberg polaritons based on electromagnetically induced transparency. *Commun. Phys.* **2021**, *4*, 101. [[CrossRef](#)]
15. Gorshkov, A.V.; Otterbach, J.; Fleischhauer, M.; Pohl, T.; Lukin, M.D. Photon-Photon Interactions via Rydberg Blockade. *Phys. Rev. Lett.* **2011**, *107*, 133602. [[CrossRef](#)] [[PubMed](#)]
16. Petrosyan, D.; Fleischhauer, M. Quantum Information Processing with Single Photons and Atomic Ensembles in Microwave Coplanar Waveguide Resonators. *Phys. Rev. Lett.* **2008**, *100*, 170501. [[CrossRef](#)] [[PubMed](#)]
17. Sedlacek, J.A.; Schwettmann, A.; Kübler, H.; Löw, R.; Pfau, T.; Shaffer, J.P. Microwave electrometry with Rydberg atoms in a vapour cell using bright atomic resonances. *Nat. Phys.* **2012**, *8*, 819–824. [[CrossRef](#)]
18. Sedlacek, J.; Schwettmann, A.; Kübler, H.; Shaffer, J. Atom-based vector microwave electrometry using rubidium Rydberg atoms in a vapor cell. *Phys. Rev. Lett.* **2013**, *111*, 063001. [[CrossRef](#)]
19. Fan, H.; Kumar, S.; Sedlacek, J.; Kübler, H.; Karimkashi, S.; Shaffer, J.P. Atom based RF electric field sensing. *J. Phys. B At. Mol. Opt. Phys.* **2015**, *48*, 202001. [[CrossRef](#)]
20. Kumar, S.; Fan, H.; Kübler, H.; Sheng, J.; Shaffer, J.P. Atom-based sensing of weak radio frequency electric fields using homodyne readout. *Sci. Rep.* **2017**, *7*, 42981. [[CrossRef](#)] [[PubMed](#)]
21. Chopinaud, A.; Pritchard, J. Optimal State Choice for Rydberg-Atom Microwave Sensors. *Phys. Rev. Appl.* **2021**, *16*, 024008. [[CrossRef](#)]
22. Anderson, D.; Sapiro, R.; Gonçalves, L.; Cardman, R.; Raitel, G. Optical Radio-Frequency Phase Measurement with an Internal-State Rydberg Atom Interferometer. *Phys. Rev. Appl.* **2022**, *17*, 044020. [[CrossRef](#)]
23. Kimel, I.; Elias, L. Relations between Hermite and Laguerre Gaussian modes. *IEEE J. Quantum Electron.* **1993**, *29*, 2562–2567. [[CrossRef](#)]
24. Nicolas, A.; Veissier, L.; Giner, L.; Giacobino, E.; Maxein, D.; Laurat, J. A quantum memory for orbital angular momentum photonic qubits. *Nat. Photonics* **2014**, *8*, 234–238. [[CrossRef](#)]
25. Trichili, A.; Rosales-Guzmán, C.; Dudley, A.; Ndagano, B.; Ben Salem, A.; Zghal, M.; Forbes, A. Optical communication beyond orbital angular momentum. *Sci. Rep.* **2016**, *6*, 27674. [[CrossRef](#)]
26. Rodrigues, J.D.; Marcassa, L.G.; Mendonça, J.T. Excitation of high orbital angular momentum Rydberg states with Laguerre–Gauss beams. *J. Phys. B At. Mol. Opt. Phys.* **2016**, *49*, 074007. [[CrossRef](#)]
27. Hamedi, H.R.; Kudriašov, V.; Jia, N.; Qian, J.; Juzeliūnas, G. Ferris wheel patterning of Rydberg atoms using electromagnetically induced transparency with optical vortex fields. *Opt. Lett.* **2021**, *46*, 4204–4207. [[CrossRef](#)]
28. Anupriya, J.; Ram, N.; Pattabiraman, M. Hanle electromagnetically induced transparency and absorption resonances with a Laguerre Gaussian beam. *Phys. Rev. A* **2010**, *81*, 043804. [[CrossRef](#)]
29. Chanu, S.R.; Natarajan, V. Narrowing of resonances in electromagnetically induced transparency and absorption using a Laguerre–Gaussian control beam. *Opt. Commun.* **2013**, *295*, 150–154. [[CrossRef](#)]
30. Chauhan, V.S.; Kumar, R.; Manchainah, D.; Kumar, P.; Easwaran, R.K. Narrowing of electromagnetically induced transparency by using structured coupling light in  $^{85}\text{Rb}$  atomic vapor medium. *Laser Phys.* **2020**, *30*, 065203. [[CrossRef](#)]

31. Akin, T.; Krzyzewski, S.; Marino, A.; Abraham, E. Electromagnetically induced transparency with Laguerre–Gaussian modes in ultracold rubidium. *Opt. Commun.* **2015**, *339*, 209–215. [[CrossRef](#)]
32. Akin, T.; Krzyzewski, S.; Holtfrerich, M.; Abraham, E. Optimization of electromagnetically induced transparency by changing the radial size of Laguerre–Gaussian laser modes. *JOSA B* **2017**, *34*, 1286–1293. [[CrossRef](#)]
33. Carr, C.; Adams, C.S.; Weatherill, K.J. Polarization spectroscopy of an excited state transition. *Opt. Lett.* **2012**, *37*, 118–120. [[CrossRef](#)] [[PubMed](#)]
34. Meyer, D.H.; Kunz, P.D.; Solmeyer, N. Nonlinear polarization spectroscopy of a Rydberg state for laser stabilization. *Appl. Opt.* **2017**, *56*, B92–B96. [[CrossRef](#)] [[PubMed](#)]
35. Corwin, K.L.; Lu, Z.T.; Hand, C.F.; Epstein, R.J.; Wieman, C.E. Frequency-stabilized diode laser with the Zeeman shift in an atomic vapor. *Appl. Opt.* **1998**, *37*, 3295–3298. [[CrossRef](#)] [[PubMed](#)]
36. Becerra, F.E.; Willis, R.T.; Rolston, S.L.; Orozco, L.A. Two-photon dichroic atomic vapor laser lock using electromagnetically induced transparency and absorption. *J. Opt. Soc. Am. B* **2009**, *26*, 1315–1320. [[CrossRef](#)]
37. Pritchard, J.D. *Cooperative Optical Non-Linearity in a Blockaded Rydberg Ensemble*; Springer Science & Business Media: Berlin/Heidelberg, Germany, 2012.
38. Virtanen, P.; Gommers, R.; Oliphant, T.E.; Haberland, M.; Reddy, T.; Cournapeau, D.; Burovski, E.; Peterson, P.; Weckesser, W.; Bright, J.; et al. SciPy 1.0: Fundamental algorithms for scientific computing in Python. *Nat. Methods* **2020**, *17*, 261–272. [[CrossRef](#)] [[PubMed](#)]
39. Harris, M.; Adams, C.; Cornish, S.; McLeod, I.; Tarleton, E.; Hughes, I. Polarization spectroscopy in rubidium and cesium. *Phys. Rev. A* **2006**, *73*, 062509. [[CrossRef](#)]
40. Do, H.D.; Moon, G.; Noh, H.R. Polarization spectroscopy of rubidium atoms: Theory and experiment. *Phys. Rev. A* **2008**, *77*, 032513. [[CrossRef](#)]
41. Su, H.J.; Liou, J.Y.; Lin, I.C.; Chen, Y.H. Optimizing the Rydberg EIT spectrum in a thermal vapor. *Opt. Express* **2022**, *30*, 1499–1510. [[CrossRef](#)]